Deep–Sea Research Part I 123 (2017) 62–74

Contents lists available at ScienceDirect

Deep–Sea Research I

journal homepage: www.elsevier.com/locate/dsri

Ocean response to typhoons in the western North Pacific: Composite results from Argo data

Sheng Lin[a,c,d], Wen-Zhou Zhang[a,b,c,d,*], Shao-Ping Shang[a,d], Hua-Sheng Hong[a,c]

[a] State Key Laboratory of Marine Environmental Science, Xiamen University, Xiamen, China
[b] State Key Laboratory of Satellite Ocean Environment Dynamics (Second Institute of Oceanography, State Oceanic Administration), Hangzhou, China
[c] Fujian Provincial Key Laboratory for Coastal Ecology and Environmental Studies, Xiamen University, Xiamen, China
[d] Key Laboratory of Underwater Acoustic Communication and Marine Information Technology (Xiamen University), Ministry of Education, Xiamen, China

ARTICLE INFO

Keywords:
Ocean response to typhoons
Composite results
Argo data
Western North Pacific

ABSTRACT

Composite structures of ocean temperature and salinity anomalies caused by tropical cyclones (TCs) or typhoons in the western North Pacific Ocean were obtained from Argo data. These structures were used to analyze ocean responses to typhoons and the dynamic mechanisms inherent in those responses with a particular focus on upwelling. TC-induced cooling is often strongly rightward-biased in the surface layer, and shifts toward the typhoon track at depths exceeding roughly 100 m. In the central water column within approximately 75 km of the typhoon track, subsurface warming predicted by vertical mixing is restrained and replaced by cooling due to upwelling. Upwelling contributes 15% on average to temperature cooling in the near surface layer (10–30 m), 84% in the subsurface layer (30–250 m) and 94% in the deep layer (250–600 m) during the period of 0.5–2.5 days after the typhoon's passage. It is suggested that the sea surface cooling effect of vertical mixing can be enhanced by the upwelling. The effect of upwelling is also prominent in the salinity response to typhoons. The composite results from the Argo data clearly reveal basic ocean responses to typhoons and indicate the important role of upwelling therein.

1. Introduction

The upper ocean response to tropical cyclones (TCs), or typhoons in the western North Pacific, has attracted considerable attention (Zhang et al., 2016) since strong air-sea interactions were identified by Emanuel (1986). Many studies have shown that TCs usually cause sea surface temperature (SST) to decrease (cooling), inducing a cold wake (e.g., Leipper, 1967; Brand, 1971; Price, 1981; Bender et al., 1993; D'Asaro et al., 2007; Wu et al., 2016). The amplitude of the cooling depends on the intensity and translation speed of the individual TC, as well as on the preceding thermal structure of the upper ocean (Price, 1981; Hart et al., 2007; Lin et al., 2008). Stronger, slower-moving, and higher-latitude TCs usually cause a larger magnitude of SST anomaly (Lin et al., 2008; Mei and Pasquero, 2013). Slowly moving TCs have relatively longer residence time to produce a stronger vertical mixing and upwelling as well as more heat loss from ocean to air (Price, 1981; D'Asaro et al., 2014). As a result, they tend to induce larger SST drop than fast moving TCs (Lloyd and Vecchi, 2011; Vincent et al., 2012b). A TC with the same translation speed and intensity causes quite smaller SST cooling under the condition with a thicker warm upper layer than it does under the climatological condition (Lin et al., 2008; Vincent et al., 2012b).

The core of the TC-induced cold wake tends to appear at the right rear corner of the typhoon in the Northern Hemisphere (Leipper, 1967; Price, 1981). On the right side, the clockwise rotation of the wind stress tends to strengthen the wind induced inertial currents and enhance the shear-induced vertical mixing (Price et al., 1994). Meanwhile, the wind speed is stronger on the right side than that on the left (Price, 1981; Mei and Pasquero, 2013). These are responsible for the rightward bias of surface cooling (Price, 1981; Price et al., 1994; Mei and Pasquero, 2013). In the subsurface layer, the temperature may increase as a result of strong vertical mixing induced by the TC (Price, 1981; Emanuel, 2001). This vertical mixing plays a dominant role in both the surface cooling and subsurface warming processes by transporting heat from the surface layer to the subsurface layer.

Because vertical mixing, or entrainment, is regarded as the most important mechanism in sea surface cooling caused by TCs (Price, 1981), the role of upwelling is usually neglected (e.g., Emanuel et al., 2004). However, some model simulations and case study analyses have demonstrated that the exclusion of upwelling may result in the underestimation of SST cooling (Yablonsky and Ginis, 2009; Chiang et al., 2011). Yablonsky and Ginis (2009) indicated that without the effect of

* Corresponding author.
E-mail address: zwenzhou@xmu.edu.cn (W.-Z. Zhang).

http://dx.doi.org/10.1016/j.dsr.2017.03.007
Received 26 August 2016; Received in revised form 6 December 2016; Accepted 16 March 2017
Available online 18 March 2017

upwelling, more than half of the storm-core sea surface cooling is neglected for TCs translating at a speed of less than 2 m s^{-1}. Chiang et al. (2011) found that the upwelling induced by Typhoon Kai-Tak accounted for 62% of the SST anomaly, double the contribution (31%) of entrainment. In the subsurface layer where the vertical gradient of temperature is large, the cooling caused by upwelling may overwhelm the warming due to vertical mixing, resulting in a subsurface cooling (Price et al., 1994). Upwelling (vertical advection) enhances the SST cooling associated with TCs, especially for slowly moving ones that can affect a location for longer time (Price, 1981; D'Asaro et al., 2014). The importance of upwelling in ocean responses to TCs remains uncertain in the statistical sense. For instance, how much does the upwelling, compared with other factors, generally contribute to the changes in temperature and salinity profiles under the influence of TCs?

Argo float data have been applied in statistically examining ocean responses to TCs in recent years (e.g., Liu et al., 2007; Park et al., 2011; Cheng et al., 2015). The observations of Argo floats showed that the passage of TCs can decrease the temperature and salinity in the mixed layer (ML) (Park et al., 2005; Liu et al., 2007). Park et al. (2011) evaluated the oceanic heat uptake associated with TCs using in situ observations from Argo floats and found that roughly 55% of Argo profile pairs did not show the expected subsurface warming. The subsurface warming occurred under strong TCs (greater than or equal to category 4) while it was not detected under weak TCs (less than or equal to category 3) (Park et al., 2011). Cheng et al. (2015) analyzed ocean thermal changes induced by TCs using Argo floats' observations. They demonstrated that TCs are responsible for 11.05 W m^{-2} annual heat transfer from the global ocean to the atmosphere just after TC passage (0–3 days) and 5.98 ± 2.1 W m^{-2} from the atmosphere to the global ocean during the period of 4–20 days after TC passage.

Many authors have used satellite remote sensing data and composite techniques to statistically analyze SST response to TCs (e.g., Hart et al., 2007; Dare and McBride, 2011; Lloyd and Vecchi, 2011; Mei and Pasquero, 2013). Hart et al. (2007) composited the mean SST response to TCs averaged over a 5°×5° box. They found that the amplitude of the SST cooling depends on TC intensity, and the rewarming of SST commonly occurs within approximately 35 days. Dare and McBride (2011) showed that the maximum SST cooling mostly occurs 1 day after TC passage; the global average SST anomaly induced by TCs is −0.9 °C; the SST of 44% data points recovers to climatological SST within 5 days and 88% within 30 days. The size of the SST cooling and the SST recovery time are affected by TC intensity and translation speed (Dare and McBride, 2011). By decomposing the responses in the along-track direction and in the across-track direction, Mei and Pasquero (2013) found that SST anomaly (SSTA) is relatively uniform along the track, and then they asserted that the spatial structure of TC-induced cold wake is a function of the distance across the TC track.

Because satellite remote sensing observations were limited to the ocean surface layer, the composite results obtained from remote sensing data described only surface ocean response to TCs (e.g., Mei and Pasquero, 2013). Although a limited number of pioneering statistical studies using Argo data focused on the ocean response (e.g., Liu et al., 2007; Park et al., 2011; Cheng et al., 2015), inadequate attention was paid on the important role of upwelling. These motivated us to statistically investigate the ocean response to typhoons using Argo profiles and improve our understanding of this issue, especially the contribution of upwelling to temperature and salinity anomalies. In this study, we attempt to examine three-dimensional mean structures of ocean temperature and salinity responses to typhoons via a composite method based on abundant Argo observation data; and we discuss the dynamic mechanisms of these responses using statistical means rather than individual cases. Additionally, we quantitatively evaluate the importance of upwelling relative to other factors in this process.

2. Data and methods

2.1. Data

Argo programme was devised in the end of last century to set up a global array of profiling floats that collect temperature and salinity profiles in the upper 2000 m of ice-free open oceans. More than 10,000 Argo floats have been deployed since 1999 and now nearly 3900 floats are operating in all oceans (Riser et al., 2016). A typical Argo float is programmed to descend to a parking depth of 1000 m. After a parking period of almost 9 days it dives to 2000 m and subsequently rises to the sea surface within about 6 h. During its ascending (occasionally descending) stage, it synchronously samples ocean properties (e.g., temperature, salinity and pressure). At the surface, it transmits these data to a satellite and then land stations before it descends to the parking depth again. The period of a complete cycle is designedly 10 days. Argo data have to pass a series of real-time quality control tests (e.g., impossible speed, pressure increasing and spike tests) within 24 h of obtainment so that they can serve as real-time data with a flag of 1 (good data), otherwise they are marked with a flag of '3' (potentially correctable bad data) or '4' (bad data). Delayed-mode quality controls are performed to further examine Argo profile data for pointwise errors using other observations such as historical data and measurements from nearby floats, and the flag set incorrectly in the real-time procedure is changed. During both real-time and delayed-mode procedures, some adjustments have been conducted if appropriate, for example, pressure adjustments for surface pressure offsets and sensor drift. Argo data only undergoing the real-time procedure are called real-time data and those experiencing these two procedures are called delayed-mode data. More detailed information about quality controls can be found in Argo quality control manual (http://www.argodatamgt.org/content/download/20685/142877/file/argo-quality-control-manual_version2.9.pdf).

Argo float data have been used in many studies addressing ocean response to typhoons, including case studies (e.g., Lin et al., 2008; Siswanto et al., 2008) and statistical analyses (e.g., Park et al., 2005; Liu et al., 2007; Park et al., 2011). Argo profile data adopted in this work were taken from the Coriolis Global Data Acquisition Center of France (Argo, 2000), covering the period from 2000 to 2012 and the area of 105°-180°E, 0°-50°N. These data include delayed-mode and real-time profiles with a quality flag of 1. To obtain composite structures, the selected Argo profiles must meet the following criteria: (1) the minimum observation depth is shallower than 10 dbar and the maximum is deeper than 700 dbar; and (2) the pressure difference between two consecutive records does not exceed 25 dbar for the 0–100 dbar layer and 50 dbar for the 100–700 dbar layer.

Typhoon data were taken from the best track dataset provided by the Joint Typhoon Warning Center, and the data include the typhoons' locations and intensity information at 6-h intervals. One climatological dataset, the Argo-only version of CARS2009, was used to establish the background ocean state. The CARS2009 was made by the Commonwealth Scientific and Industrial Research Organization and distributed in July 2009. It covers global oceans mapped on a 1/2° longitude-latitude grid mesh. Vincent et al. (2012a) thought that during the period of 3–10 days before a storm approaching, the ocean state was not affected by the storm and could be taken as pre-storm condition. The average temperature and salinity profiles obtained from the Argo data during 3–10 days before a typhoon approaching are almost consistent with those from the CARS2009 dataset (Fig. 1), with a small mean bias of 0.085 °C for temperature and 0.0026 psu for salinity (the latter minus the former). There is an obvious bias of up to 0.02 psu in the upper 30 m layer between the climatological salinity values and the Argo data. The bias profiles of temperature and salinity were subtracted from the corresponding climatological profiles. These corrected climatological data served as pre-typhoon models in this work.

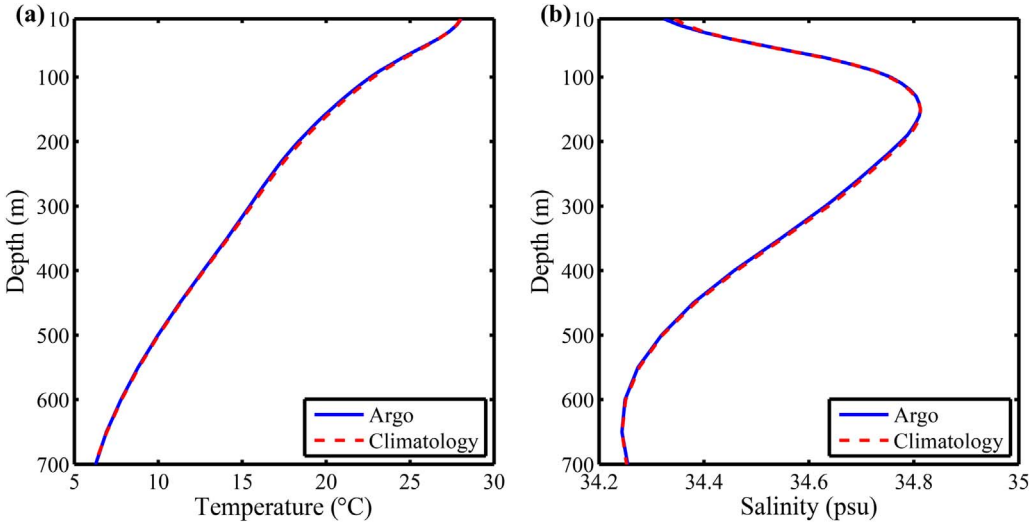

Fig. 1. Comparision of averaged temperature and salinity profiles between climatological data and Argo floats' observations obtained during the period of 3–10 days prior to TC passage within 500 km of the TC track (see Fig. 2c).

2.2. Methods

For a given typhoon, two parameters for each selected profile were determined: the shortest cross-track distance (Dm km) to the typhoon track and the time period (Td, rounded to integer days) between Argo profiling time and the time as the typhoon center passes the point nearest to the profiling location (referred to as the nearest point). Actually, the nearest point is just located at the intersection point of the typhoon track and the cross-track line that passes the profile and is perpendicular to the typhoon track. If such a cross-track line is non-existing for an Argo profile, this profile has no cross-track distance and will not be considered for the typhoon. Positive (negative) distance relates to the right (left) side of the typhoon track looking in the direction toward which the typhoon moved. Positive (negative) period means that Argo float profiled after (before) the typhoon passed the nearest point. Only profiles with −500 km≤Dm≤500 km and −10 days≤Td≤50 days were kept for the given typhoon. Simultaneously, the intensity and translation speed of the typhoon at the nearest point to each Argo profile were recorded as the typhoon conditions corresponding to the Argo profile. After checking all typhoons during 2000–2012 in the same way, there were 19537 Argo profiles kept for the following composing procedure, together with their corresponding typhoon conditions. The distribution of typhoons and Argo profiles used in this study is shown in Fig. 2. The pre-typhoon oceanic state at each profiling location was obtained via spatial interpolation from the climatological data field on the same day of the year as the profile. Both the Argo profile and corresponding pre-typhoon oceanic state data were interpolated to standard levels (depths) at a 10 m interval beginning at 10 m depth. Temperature and salinity anomalies were calculated for every 10 m depth value by subtracting the pre-typhoon oceanic state from the Argo data. Finally, the temperature and salinity anomaly profiles with the same time period were separately interpolated to cross-track grids ranging from −500 to 500 km at 10 km intervals via an optimal interpolation method (Gandin, 1965). The above method determined the composite structures of the oceanic response to typhoons, which were mapped on grids at 10 km intervals in the cross-track direction at a temporal interval of one day for each standard level from 10 to 700 m depth.

Note that Argo observations may contain signals of significant background variability (such as seasonal cycle, baroclinic fronts and mesoscale eddies) that is independent of TC activity (Park et al., 2011). Both the Argo observations and the climatological data include large scale of seasonal, spatial background signals. When temperature and salinity anomalies for each Argo profile were obtained from the difference between the Argo observations and the climatological data at the same location on the same day of the year, the large-scale component of background variability was eliminated. Short-term and small-scale component could be smoothed by the interpolating procedure mentioned above in the composite method. Thus, the influence of background variability in this composite method is limited, compared with strong signals of ocean response to TCs.

Based on the heat and salt budget equations (Price et al., 1994), we calculated the temperature and salinity anomalies caused by upwelling using the following formulas:

$$\Delta T_U = \int_0^t \left(w\frac{\partial T}{\partial z}\right)dt = \overline{\frac{\partial T}{\partial z}}\int_0^t w dt = \overline{\frac{\partial T}{\partial z}}\Delta H_t, \quad (1)$$

$$\Delta S_U = \int_0^t \left(w\frac{\partial S}{\partial z}\right)dt = \overline{\frac{\partial S}{\partial z}}\int_0^t w dt = \overline{\frac{\partial S}{\partial z}}\Delta H_t, \quad (2)$$

where the time-averaged vertical gradient of temperature $\left(\overline{\frac{\partial T}{\partial z}}\right)$ was approximately estimated from the mean profile of climatological temperature profile (representing the value at time t=0) and Argo temperature profile (the value at time t), and so was the time-averaged vertical gradient of salinity $\left(\overline{\frac{\partial S}{\partial z}}\right)$. In order to estimate the role of vertical advection in the heat budget of the upper ocean, Large et al. (1986) assumed that the vertical velocity is constant below the ML and then falls linearly to zero at the surface. Following Large et al. (1986), we assumed that the amplitude of upwelling (time integration of vertical velocity w, ΔH_t) is constant below the ML, and then falls linearly to zero at the surface. In this study, we took the displacement of the 14 °C isotherm (observed by Argo floats) with respect to its location in the climatological temperature profile as the amplitude of upwelling bellow the ML, following Price et al. (1994). The mean depth of this isotherm in the study region is 367 m with the standard deviation of 88 m. From 0.5 to 2.5 days after the typhoon passage, the 14 °C isotherm rises up approximately 18.2 m within 75 km of the typhoon track. Based on the values of ΔT_U and ΔS_U, we could determine the contribution of upwelling to typhoon-induced total temperature and salinity anomalies in each depth.

3. Results and discussion

3.1. Evolution of temperature and salinity anomalies

The mixed layer depth (MLD) is much deeper than 10 m under the

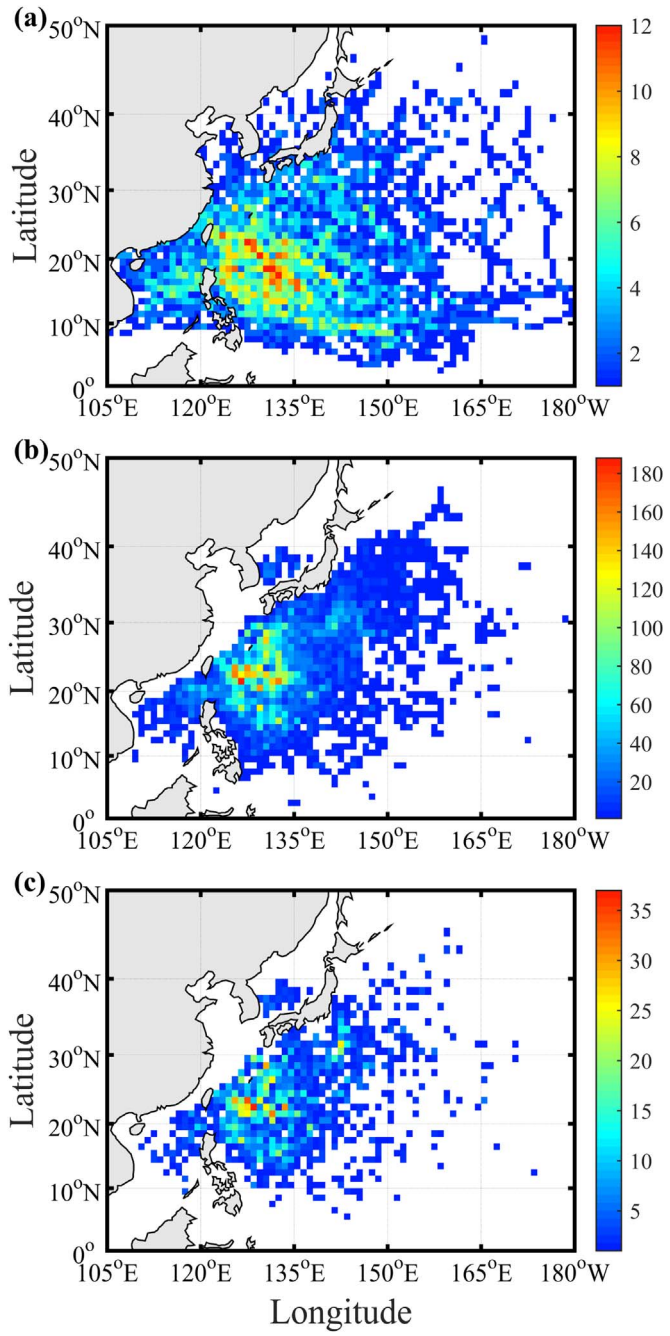

Fig. 2. (a) Number of TCs in the study region. TCs without corresponding Argo observations are not included. (b) Number of Argo profiles during the period from 3 days before TC passage to 50 days after TC passage. (c) Number of Argo profiles during the period from 10 to 3 days before TC passage. In every panel, the number in each 1°×1° box is the result during 2000–2012.

influence of a TC and the vertical gradients of temperature and salinity are very weak in the ML (Liu et al., 2007; Price, 2009). We estimated the MLD using a threshold of 0.2 °C temperature difference between the values at the 10 m depth and at the base of the ML, following de Boyer Montégut et al. (2004) who used Argo data to investigate the ML physics over the global ocean. On average, the MLD is 52.9 m and the vertical gradient of temperature (salinity) in the layer of 10–20 m is only 0.0088 °C m^{-1} (−0.0007 psu m^{-1}) based on Argo observations under the influence of typhoons. Therefore, the difference between SST or sea surface salinity (SSS) and the corresponding value at the 10 m depth (near surface) must be negligible in this work. We denoted the temperature and salinity at the 10 m depth by SST and SSS for simplicity, respectively, since there were no surface data in Argo observations.

Fig. 3a shows that the SST begins to decrease about one day before typhoon arrival. SST cooling then rapidly intensifies until one day after typhoon passage, when it reaches a maximum anomaly of about −2.31 °C. With the advent of abundant satellite observations, many studies have focused on SST cooling (e.g., Hart et al., 2007; Mei and Pasquero, 2013). Using satellite remote sensing data, Mei and Pasquero (2013) found that their composite SST anomaly peaked during the day following TC passage. Subsequently, SST increases slowly and the SST anomaly decreases. SST cooling results in a cold wake and its core clearly appears on the right side of the typhoon track (Mei and Pasquero, 2013). Price (1981) hypothesized that this rightward shift is primarily caused by the clockwise turning wind-stress on the right side of the TC track, which is approximately resonant with the velocity in the ML.

The cold wake lasts for over 25 days before returning to normal conditions (Fig. 3a). In order to determine the recovery time of the SST from cooling, the change of the SST anomaly (SSTA) during the thirty days after the typhoon passage could be described using the following formula, obtained via a nonlinear least-square fitting method (Fig. 4c):

$$SSTA(t) = -1.27\exp\left(-\frac{t}{8.63}\right) - 0.127. \quad (3)$$

The e-folding recovery time is approximately 8.6 days and the 95% confidence range is 6.42–13.15 days. These results are in good agreement with previous observational and modeling studies (e.g., Price et al., 2008; Dare and McBride, 2011; Mei and Pasquero, 2012; Bueti et al., 2014). Case studies by Price et al. (2008) demonstrated that the e-folding recovery time of the cold wake induced by a moving hurricane is 5–20 days. The cold wake almost disappears in 30 days after the typhoon passage, although the SSTA derived by the above formula remains infinitely close to −0.127 °C (Fig. 4). Based on model simulations and remote sensing observations, Vincent et al. (2012a) showed that the surface cooling is insignificant approximately 40 days after a TC's passage in spite of a small SSTA of −0.2 °C relative to pre-storm conditions.

Fig. 4a shows that a negative temperature anomaly extends to the depth greater than 500 m after typhoon passage. Subsurface cooling (denoted by the results at 100 m depth) begins about one day before a typhoon's arrival and becomes strongest one day after maximum surface cooling occurs. Subsequently, subsurface cooling weakens. A distinct negative temperature anomaly lasts for more than 8 days (Fig. 3b). This trend extends beyond the typhoon track to a width of approximately 200 km, which is obviously narrower than the width (more than 400 km) of the surface cooling (Fig. 3a and b). Recently, the cooling below the surface has been observed during several TCs (e.g., Sanford et al., 2011; Mrvaljevic et al., 2013; D'Asaro et al., 2014).

Two positive temperature anomaly strips appear on both sides of the subsurface cooling area, particularly in the layer of 50–200 m (Fig. 3b). This subsurface warming occurs in a series of peaks, which is also evident in Fig. 4a during the period after the subsurface cooling has faded away. A similar phenomenon can be observed in the salinity anomaly also (Fig. 4b). The power spectrum of the mean temperature anomaly, which covers the period from 4 to 30 days, indicates a significant peak at the 0.22 cycles per day (cpd) frequency (95% significance level, Fig. 3d). Many studies have reported that TCs can trigger near-inertial oscillations (e.g., Price, 1983; Price et al., 1994). Given that the inertial frequency is approximately 0.782 cpd at the average latitude (23°N) of Argo profiles, the energy at this frequency will be folded back to the 0.218 cpd frequency due to the 1 day data sampling interval (Emery and Thomson, 2001), which is in agreement with the results presented here. To test the sensitivity of the above conjecture to data used, 90% of total Argo profiles were randomly extracted six times and the same analyses were conducted separately

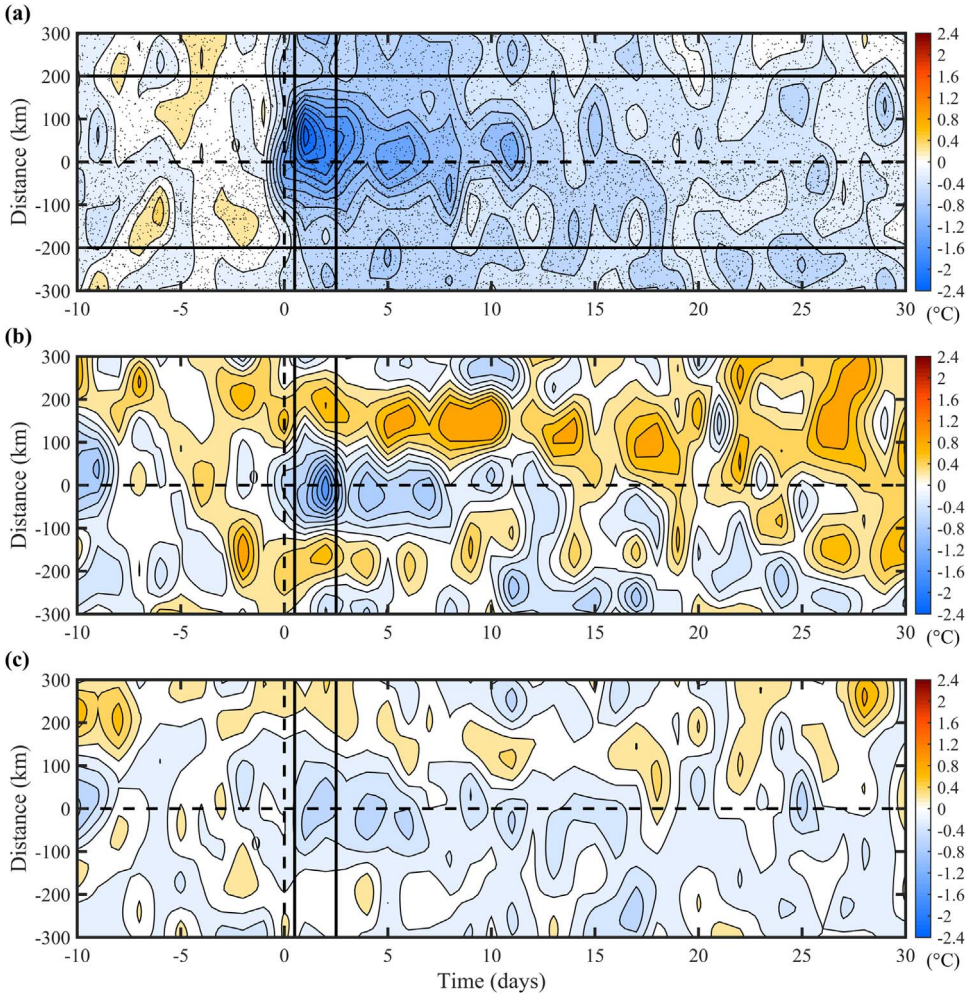

Fig. 3. The evolution of composite temperature anomaly at (a) 10 m, (b) 100 m and (c) 400 m depths, under the influence of typhoons. Time on the abscissa axis denotes the days relative to the passage of a typhoon's center (negative means before the typhoon's arrival and positive means after the typhoon's passage). The positive (negative) value on the ordinate axis is the distance to the right (left) of the typhoon track, looking in the direction of the typhoon's motion. The contour interval is 0.2 °C. Black points in (a) denote the locations of all Argo profiles used in this work. The results between the two horizontal black solid lines were applied to calculate the evolution of the cross-track averaged temperature anomaly profile (Fig. 4a) and those between the two vertical black solid lines were adopted to obtain a cross-track vertical structure of temperature response (see Figs. 5a and 6).

for these six groups of sub-sampled Argo profiles. An evident signal appears at almost the same frequency mentioned above in each group of data. When we changed time step from 1 day to 0.64 day (about half an inertial period at 23°N), a result similar to Fig. 4a was obtained (figure omitted). Thus, the periodic variations in the subsurface temperature anomaly are likely associated with near-inertial oscillations as observed by Sanford et al. (2011) and Mrvaljevic et al. (2013).

3.2. Vertical structures across a typhoon track

To examine the vertical structures of temperature and salinity anomalies, we analyzed a cross-track transect (shown in Fig. 3) averaged between day 0.5 and day 2.5 after a typhoon's passage. This transect describes the strongest ocean response to a typhoon. Fig. 5a and d show the along-track mean vertical structures of temperature and salinity anomalies, respectively.

In Fig. 5a, a maximum negative SST anomaly of −2.09 °C appears approximately 60 km to the right of the typhoon track. This rightward bias extends to a depth of 50 m and gradually narrows toward the typhoon track as depth increases. At 50 m depth, the temperature anomaly, which exceeds −0.4 °C, is only 200 km wide, while at the surface it extends over 600 km. Below the 50 m layer, the strong rightward bias in the cooling disappears. Another weak cooling core exists at a depth of 80 m. As indicated by the −0.2 °C contour, the negative temperature anomaly penetrates more than 600 m deep.

Below 50 m, the temperature anomaly is positive (warming) on both sides of the central cooling mass (Figs. 5a and 6). There are two warming cores: one at approximately 210 km to the right of the typhoon track and the other at 170 km to the left. They are located at a depth of 70–100 m. The right warming core is stronger than the left core, indicating that the mechanism of its formation is shear-induced vertical mixing.

Fig. 5d shows the cross-track structure of the composite salinity anomaly associated with an average typhoon. A significant positive salinity anomaly appears in the surface layer, coincident with the negative temperature anomaly. The core of the positive salinity anomaly, which has a maximum 0.10 psu, is approximately 230 km to the right of the typhoon track. Similar to the negative temperature anomaly, the positive salinity anomaly also narrows toward the track with depth, and another positive salinity anomaly core is produced to the left of the track at approximately 50 m deep. The difference between the temperature and salinity anomalies is that the positive salinity anomaly is limited to the layer above 120 m. Below the positive anomaly is negative salinity anomaly extending from 120 m to nearly 600 m under the typhoon track.

A strong negative salinity anomaly core with a minimum −0.11 psu is generated by vertical mixing, which locates approximately 100 km to the right of the typhoon track in the subsurface layer from 70 to 80 m deep,

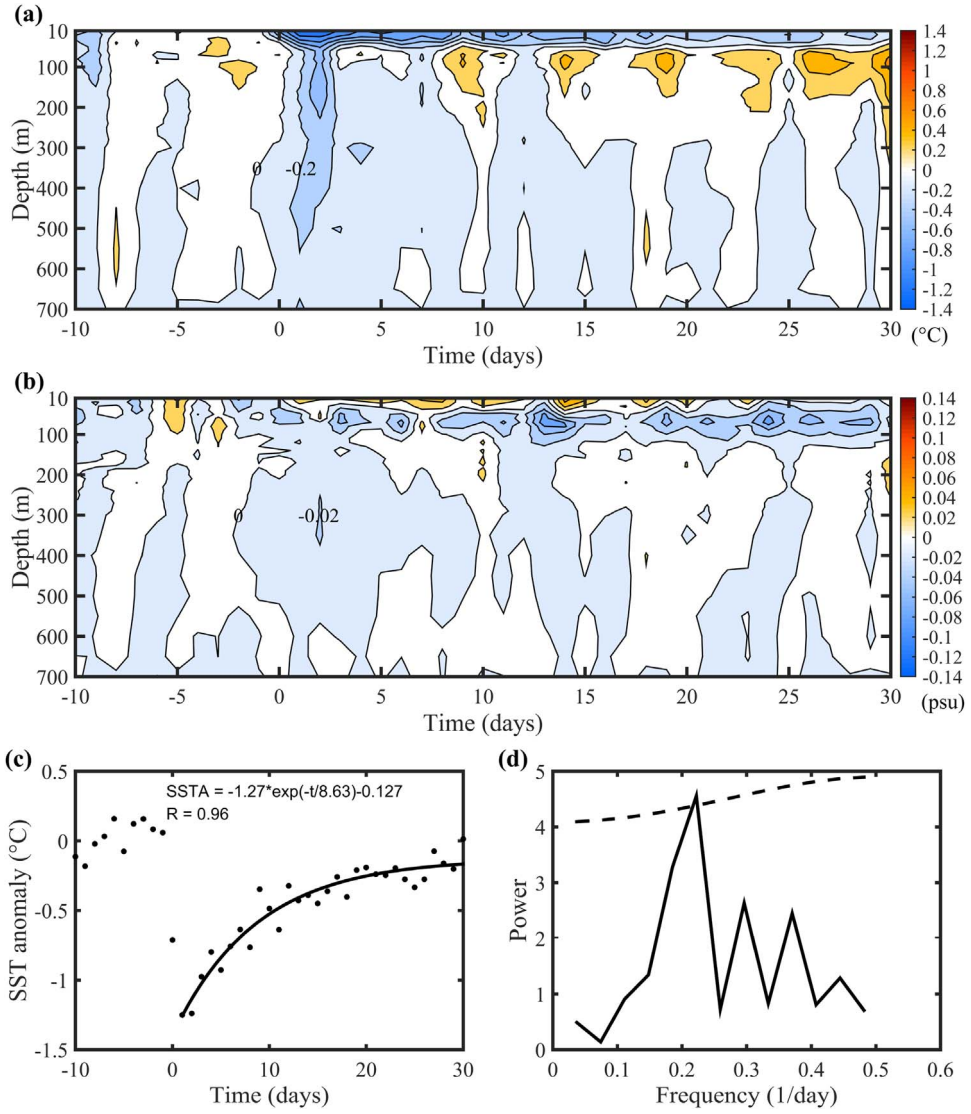

Fig. 4. Temporal evolution of cross-track averaged composite anomaly profile for (a) temperature and (b) salinity. The spatial range of salinity data used is the same as that of temperature, presented in Fig. 3a. The contour intervals in (a) and (b) are 0.2 °C and 0.02 psu, respectively. (c) SST anomaly (SSTA) changes with time (t) after the typhoon's passage, fitted by a solid curve. The fitting equation is presented with a correlation coefficient (R) of 0.96. (d) Power spectrum of depth-averaged temperature anomaly in the layer of 50–200 m (solid curve). Dashed curve shows the 95% confidence level of the power spectrum.

just below the surface positive anomaly layer (Fig. 5d). At 100–200 km to the left of the track, a weak negative salinity anomaly core is located at the same depth (Fig. 5d). This negative anomaly expands to the surface layer, which may be related to rainfall. Wingo and Cecil (2010) demonstrated a leftward bias in precipitation associated with TCs using results composited from passive-microwave satellite rain rates.

In the central water column (within 75 km of the typhoon track), a negative temperature anomaly extends from the sea surface to 600 m deep (Fig. 5a and b), beyond where shear-induced vertical mixing can reach (Price, 2009). Price (2009) suggested that a typical depth of vertical mixing by a category 3 is 100 m. This suggests that, in addition to vertical mixing, upwelling plays an important role in the temperature changes of the central water column along a typhoon's path. Upwelling not only produces a negative temperature anomaly in the depths but also suppresses warming caused by vertical mixing in the subsurface, eliminating the impact of subsurface warming under the typhoon track (Figs. 5a, b, and 6). Additionally, upwelling can enhance surface cooling even though the vertical temperature gradient is weak within the surface layer. The effect of upwelling can also be observed in the structure of the salinity anomaly (Fig. 5d and e). A positive salinity anomaly produced by upwelling must be limited to ~150 m deep as shown in Fig. 5d and e because the maximum value of the climatological mean salinity profile is located at approximately 150 m (Fig. 1b). The positive effect of upwelling overcomes the negative effect of vertical mixing in the subsurface, resulting in a significant positive salinity anomaly core at approximately 60 m deep (Fig. 5d). Furthermore, upwelling causes a negative salinity anomaly below the maximum climatological salinity value, where salinity decreases slowly with increasing depth (Fig. 1b).

In open oceans, temperature and salinity anomalies due to typhoons are mainly caused by vertical mixing, upwelling, horizontal advection, and surface heat and freshwater fluxes (Price, 1981; Huang et al., 2009; Wingo and Cecil, 2010). As shown in Fig. 6, vertical mixing has been identified intuitively from temperature change and is dominant in the ML, while upwelling is the main factor affecting temperature and salinity values at deeper water levels (Price et al., 1994). However, the relative importance of upwelling in temperature and salinity responses to typhoons has not yet been statistically evaluated from observations.

Fig. 5b and e show the contributions of both upwelling and other factors to the temperature and salinity anomalies in the central water column, respectively. In the near surface layer of 10–30 m, upwelling

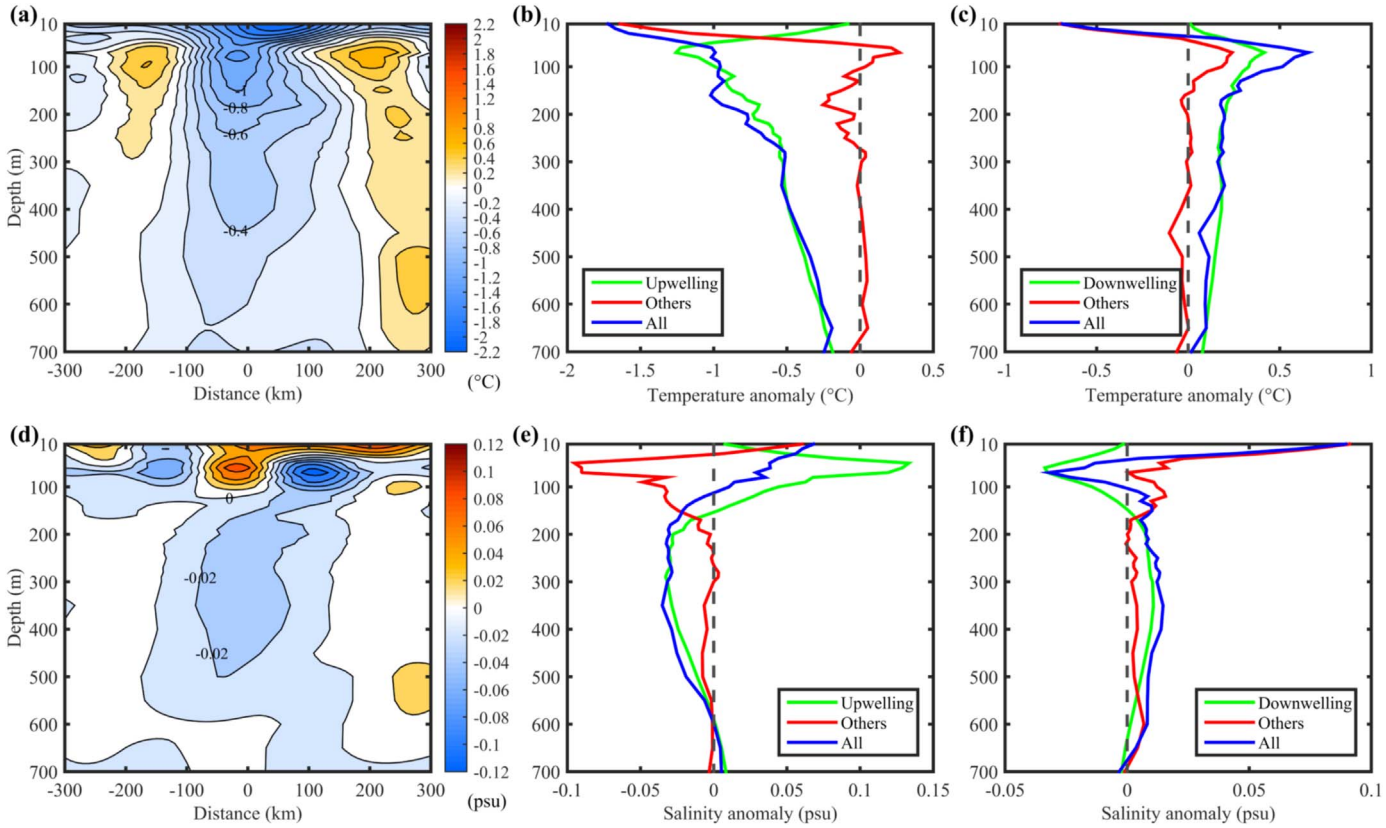

Fig. 5. Cross-track structures averaged from day 0.5 to day 2.5 after a typhoon's passage: (a) temperature anomaly and (d) salinity anomaly; the vertical profiles of (b) temperature anomaly and (e) salinity anomaly associated with upwelling and other factors averaged within 75 km of the track; the vertical profiles of (c) temperature anomaly and (f) salinity anomaly associated with downwelling and other factors averaged within 150–250 km to the right of the track. The contour intervals in (a) and (d) are 0.2 °C and 0.02 psu, respectively. All in (b), (c), (e), and (f) represents the total anomaly derived from Argo data with respect to climatological data; Upwelling (Downwelling) means the anomaly associated with upwelling (downwelling); Others denotes the anomaly associated with other factors (subtracting Upwelling or Downwelling from All).

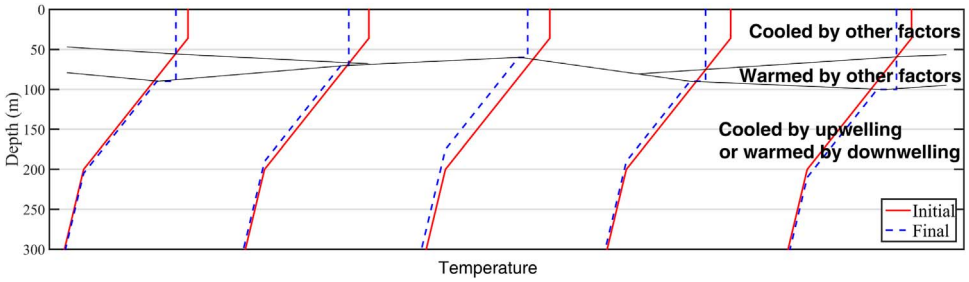

Fig. 6. Schematic diagram of oceanic temperature response to a typhoon in a cross-track section, updated from Price (1981). Temperature profiles are located at −200, −100, 0, +100, +200 km from left to right.

causes a smaller negative temperature anomaly than other factors (Fig. 5b), accounting for approximately 15% (0.25 °C vs. 1.66 °C) of the total change in temperature. Upwelling dominates the temperature anomaly below the 30 m depth (Fig. 5b). Between 30 and 250 m, on average, upwelling accounts for 84% (0.85 °C vs. 1.01 °C). In the deeper layer from 250 m to 600 m, the negative temperature anomaly induced by upwelling tends to decrease with depth due to the reduction in the temperature's vertical gradient (Figs. 5b and 1a). Nevertheless, upwelling still has a large effect on the temperature anomaly in this layer, explaining more than 94% (0.44 °C vs. 0.47 °C) of the temperature change.

The effect of upwelling on typhoon-induced temperature and salinity anomalies depends on the vertical gradients of temperature and salinity, respectively. The salinity profile is more complex than the temperature profile. Fig. 1 shows that temperature drops homogenously with depth, while salinity increases above 150 m and decreases from 150 m to 650 m deep. As a result, the contribution of upwelling to the salinity anomaly is somewhat different from that to the temperature anomaly. The salinity anomaly in the central water column is positive in the layer form 10 to 110 m. and negative below 110 m (Fig. 5d and e). Similar to the effect on temperature anomaly, upwelling causes a smaller positive salinity anomaly than other factors in the central water column from 10 m to 20 m (Fig. 5e), contributing 27% (0.017 psu vs. 0.064 psu) to the change in salinity. This layer (10–20 m) is thinner than the similar layer (10–30 m) for temperature anomaly. The possible reason for this is that the heat flux tends to enhance the temperature anomaly caused by vertical mixing in the surface and near surface layers while the rainfall tends to weaken the salinity anomaly caused by vertical mixing (Price, 1981; Wingo and Cecil, 2010). In the layer from 20 to 110 m, upwelling causes a positive salinity anomaly (0.080 psu) and dominates over the combined negative effect (−0.048 psu) of other factors on the salinity anomaly, therefore, the final salinity anomaly induced by the typhoon is positive in this layer (Fig. 5e). In the layer from 110 m to 160 m, the effect of upwelling decreases with depth because of the reduction of vertical

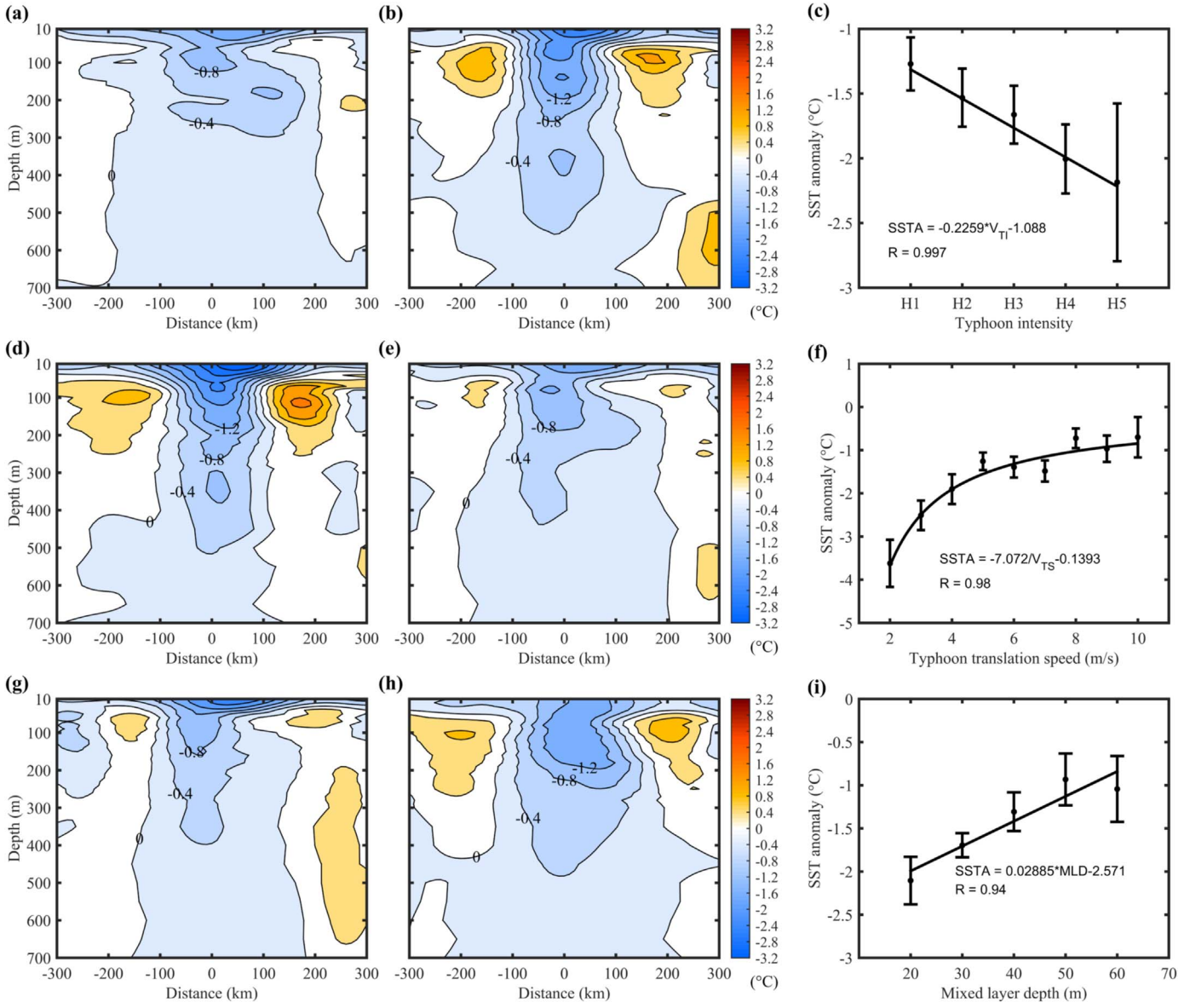

Fig. 7. Cross-track structure of temperature anomaly induced by a typhoon with: (a) weak intensity (categories 1 and 2); (b) strong intensity (categories 3–5); (d) low translation speed (≤4 m s^{-1}); (e) high translation speed (> 4 m s^{-1}); (g) above shallow ML (pre-typhoon MLD≤50 m); (h) above deep ML (pre-typhoon MLD > 50 m). The spatial range of data is presented in Fig. 3. The contour interval is 0.4 °C. (c) SST anomaly (SSTA) versus typhoon intensity, (f) SSTA versus typhoon translation speed, and (i) SSTA versus MLD. The thick solid lines or curves in (c), (f), and (i) are the fitting lines with the corresponding regression equation and R presented at a significance level of 99.9% for (c) and (f), and 98% for (i). The SSTA in (c), (f) and (i) is averaged within 100 km of the typhoon track. The error bars are calculated by dividing the corresponding standard deviations by the square root of the number of Argo profiles, following Mei and Pasquero (2013).

salinity gradient. Below this layer, upwelling becomes the dominant mechanism of salinity change, as the impact of the other factors diminishes rapidly with depth (Fig. 5e). On average, the upwelling contributes 81% (0.017 psu vs. 0.021 psu) of salinity anomaly below the 160 m depth.

Beyond the central typhoon-affected water column (≥150 km to the typhoon track), both temperature and salinity anomalies are positive below 150 m depth (Fig. 5a, c, d and f), suggesting that a downwelling phenomenon very likely occurs there (Fig. 6). Previous numerical studies have indicated that at some distance away from a hurricane track, a compensating downwelling is expected to cause warming within the thermocline (Price, 1981; Price et al., 1994). Our study indicates that a weak warming due to this downwelling extends to more than 600 m deep, as shown in Fig. 5a. It is clear in Fig. 5a that a left-right asymmetry also appears in the deep warming due to downwelling, i.e., the warming on the right side is more significant and penetrates deeper.

4. Sensitivity of temperature and salinity anomalies' vertical structures

Ocean temperature and salinity responses to typhoons depend on the intensity and translation speed of the typhoons and on pre-typhoon oceanic conditions such as the MLD (Vincent et al., 2012a, 2012b). In order to confirm the sensitivity of the average temperature and salinity anomalies' vertical structures to these parameters, we separately classified all typhoons (146) into weak (categories 1 and 2) and strong (categories 3–5) typhoons, as well as slow (translation speed ≤4 m s^{-1}) and fast (translation speed > 4 m s^{-1}) typhoons. In addition, we studied the effect of shallow (pre-typhoon MLD ≤50 m) and deep (pre-typhoon MLD > 50 m) MLs. The methods used to calculate results are the same as in Subsection 3.2. It is clear that the basic temperature anomaly pattern for each category of typhoon is similar to that for all typhoons (Figs. 7 and 5a) and so is the basic pattern of salinity anomaly (Figs. 8 and 5d). Significant differences exist in the magnitudes of the

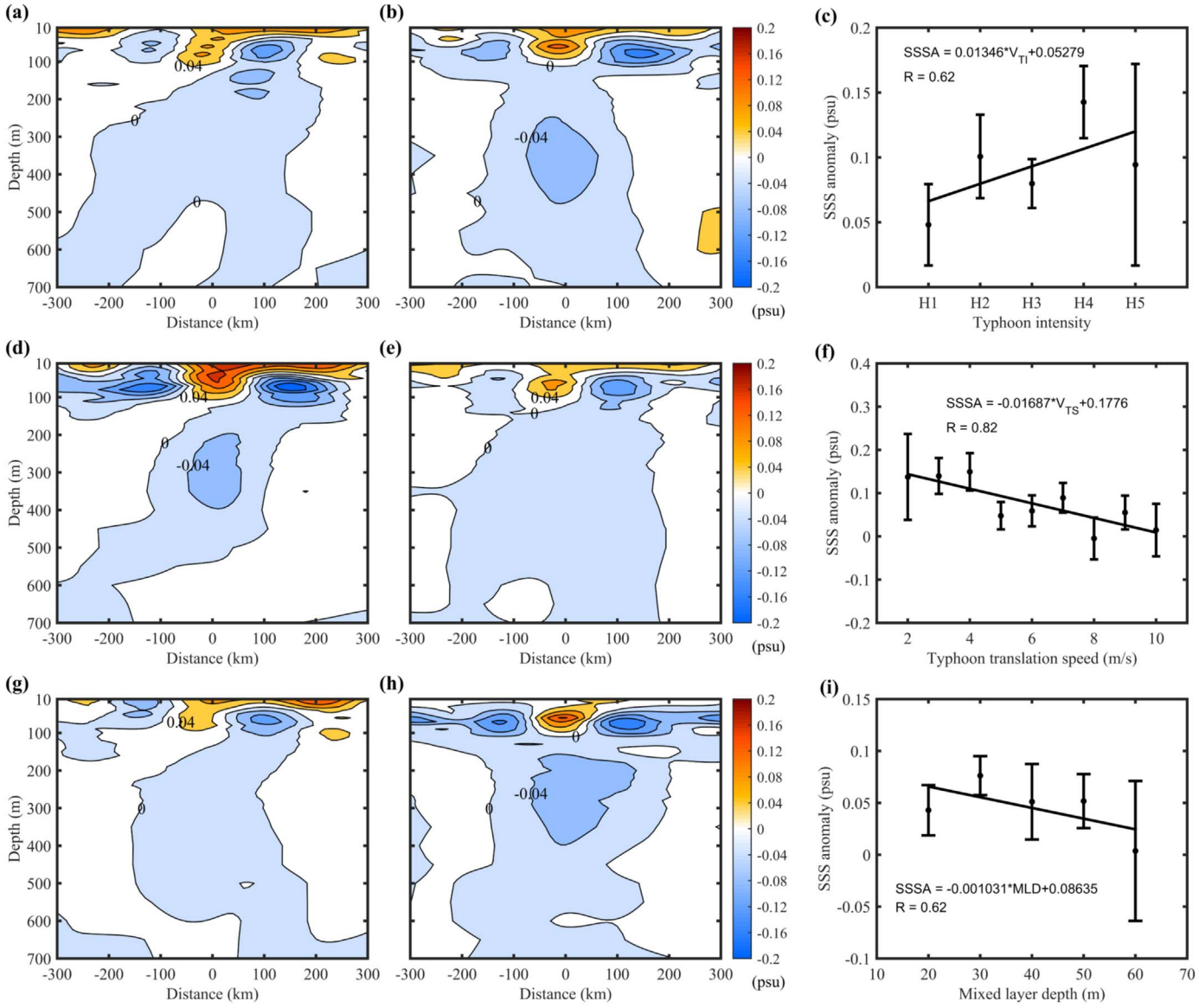

Fig. 8. Same as Fig. 7, but for salinity anomaly. The contour interval is 0.04 psu.

temperature and salinity anomalies.

Temperature and salinity values change less in response to weak typhoons when compared to strong ones, as shown in Figs. 7a, b, 8a, and b. The largest temperature anomaly induced by a strong typhoon at the 10 m depth is −2.48 °C, while that induced by a weak typhoon is only −1.62 °C. The amplitude of the temperature anomaly increases with increasing typhoon intensity along the Saffir-Simpson scale (Fig. 7c). The correlation coefficient (R) between the absolute temperature anomaly and the typhoon intensity is 0.997 (99.9% significance level). Lloyd and Vecchi (2011) have shown that the relationship between sea surface cooling and cyclone intensity is nonmonotonic and that SST cooling becomes stronger as cyclone intensity increases for hurricanes up to category 2 but becomes weaker or keeps unchanged for hurricanes beyond category 2. However, this nonmonotonic relationship occurs only for slowly moving cyclones, while for rapidly moving cyclones the SST cooling tends to intensify linearly as cyclone intensity increases (Lloyd and Vecchi, 2011). Our results demonstrate that typhoon translation speed has a much larger impact on surface cooling when typhoons move slowly (Fig. 7d). Thus, it can be concluded that the relationship between SST cooling and cyclone intensity is readily distorted by the impact of translation speed of slowly moving cyclones, but it is rarely affected by that of fast-moving cyclones. All slow and fast typhoons were included in our composite results for weak and strong typhoons so that the impact of translation speed was substantially diluted. As a result, a nearly linear relationship between SST cooling and typhoon intensity was obtained, as shown in Fig. 7c. Mei and Pasquero (2013) also suggested that a nearly linear relationship between the amplitude of SST cooling and typhoon intensity is expected when other factors such as translation speed are fixed. More uncertainty exists for stronger typhoons, as indicated by larger error bars (Fig. 7c).

On average, the 14 °C isotherm shifts upward 19.5 m (10.7 m) in association with strong (weak) typhoons. The negative temperature anomaly below the ML in the region near the typhoon track penetrates deeper and increases in magnitude during strong typhoons (Fig. 7b) when compared to weak typhoons (Fig. 7a). This implies that the former causes a stronger upwelling. Strong typhoons produce two prominent positive temperature anomaly cores in the subsurface layer of the region far from the typhoon track, indicating strong vertical mixing (Fig. 7b). By contrast, there are no such positive anomaly cores induced by weak typhoons (Fig. 7a). Similar discrepancies are also observed in the salinity response (Fig. 8a and b).

The translation speed of a typhoon determines the exposure time of the local sea surface to the typhoon's effects, which influences the

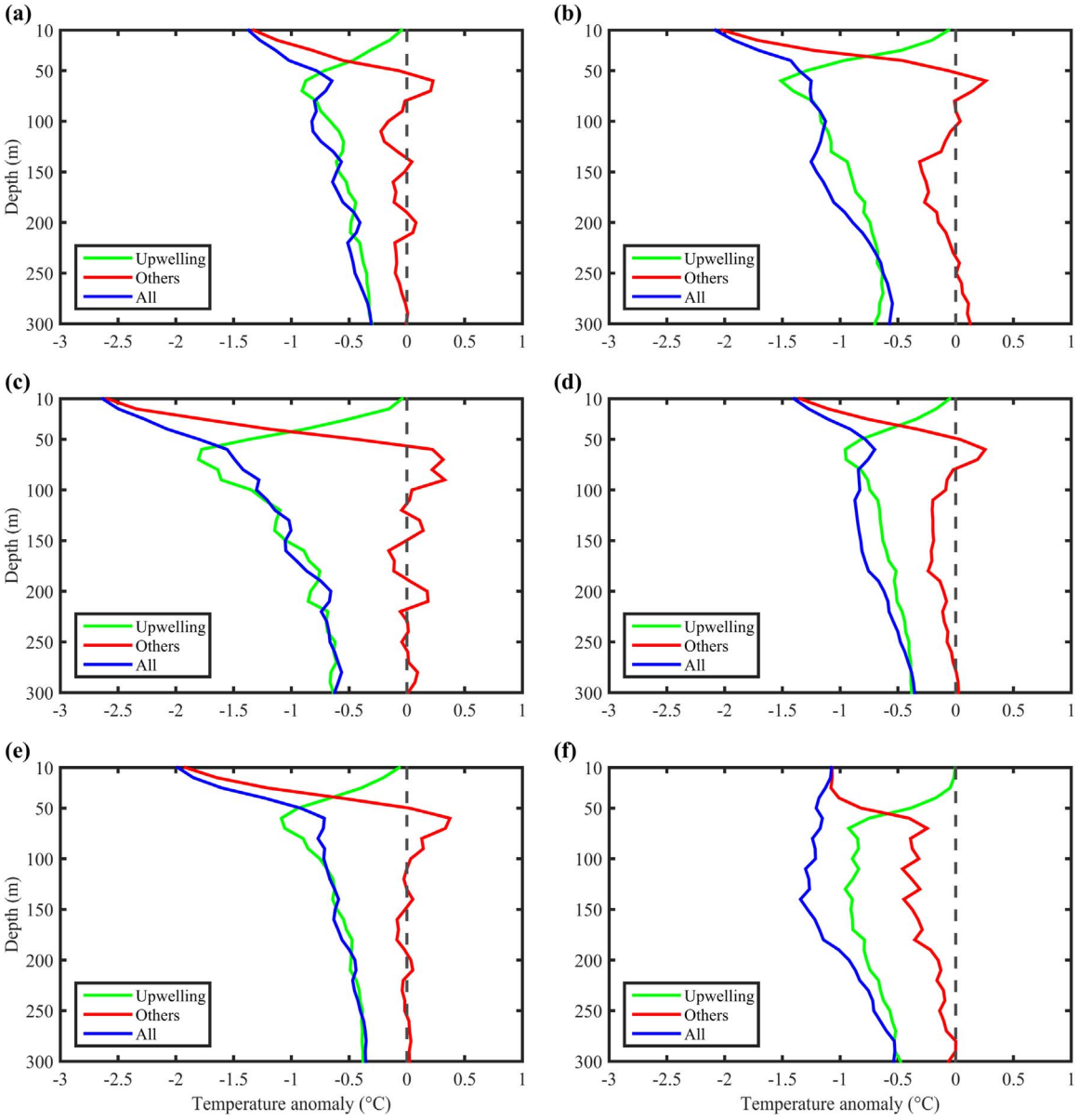

Fig. 9. The vertical profiles of temperature anomaly associated with upwelling and other factors under the influence of a typhoon with: (a) weak intensity; (b) strong intensity; (c) low translation speed; (d) high translation speed; (e) above shallow ML; (f) above deep ML. The profiles are averaged within 75 km of the typhoon track.

intensity of the ocean's response (Lin et al., 2008). Fig. 7d shows that under the influence of a slowly moving typhoon, the largest temperature anomalies in the surface layer and in the subsurface layer are −3.11 °C and 1.73 °C, respectively. These values are larger than their counterparts (−1.60 °C, 0.52 °C) associated with rapidly moving typhoons (Fig. 7e). The magnitude of negative temperature anomaly at the 10 m depth decreases nonlinearly as typhoon translation speed increases (Fig. 7f) and this relationship is more prominent for slowly moving typhoons than for rapidly moving typhoons. Similarly, the magnitude of salinity anomaly tends to decrease with typhoon translation speed (Fig. 8d–f). Slowly moving typhoons can induce stronger upwelling than rapidly moving ones because of the increased amount of time they spend along the sea surface. The former causes the 14 °C isotherm to rise up 19.7 m, compared to a 12.5 m rise caused by the latter, and results in more significant temperature and salinity anomalies (Figs. 9c, d, 10c, and d). Previous studies demonstrated that upwelling significantly enhances the SST response to a slowly moving hurricane rather than a rapidly moving one (e.g., Price, 1981; Mei and Pasquero, 2013), which is consistent with our composite results.

By comparing Fig. 7g with Figs. 7h and 8g with Fig. 8h, we can see that the typhoon above the shallow ML causes a larger negative temperature anomaly and positive salinity anomaly in the surface layer than the one above the deeper ML. The magnitude of the SSTA decreases as the MLD increases (Fig. 7i). The R-value between the negative SSTA and the MLD is 0.97 (99.9% significance level). This indicates that the pre-typhoon MLD heavily modulates the impact of vertical mixing on the temperature and salinity responses in the upper ocean. A plausible mechanism for the differing responses above is that typhoon-induced entrainment mixes warm, low-salinity water from the surface layer with cold, high-salinity water from below more easily in the shallow ML than in the deep ML (Vincent et al., 2012b). These support the result of numerical experiments by Price (1981) that the SST response is large when the initial ML is shallow with a sharp temperature gradient beneath the ML. In the subsurface layer, the case is the opposite. Larger temperature and salinity anomalies occur in the subsurface layer with the deep ML than with the shallow ML (Figs. 7g, h, 8g, and h). The possible reason for these differing responses is the systematic difference in the translation speeds of the different category

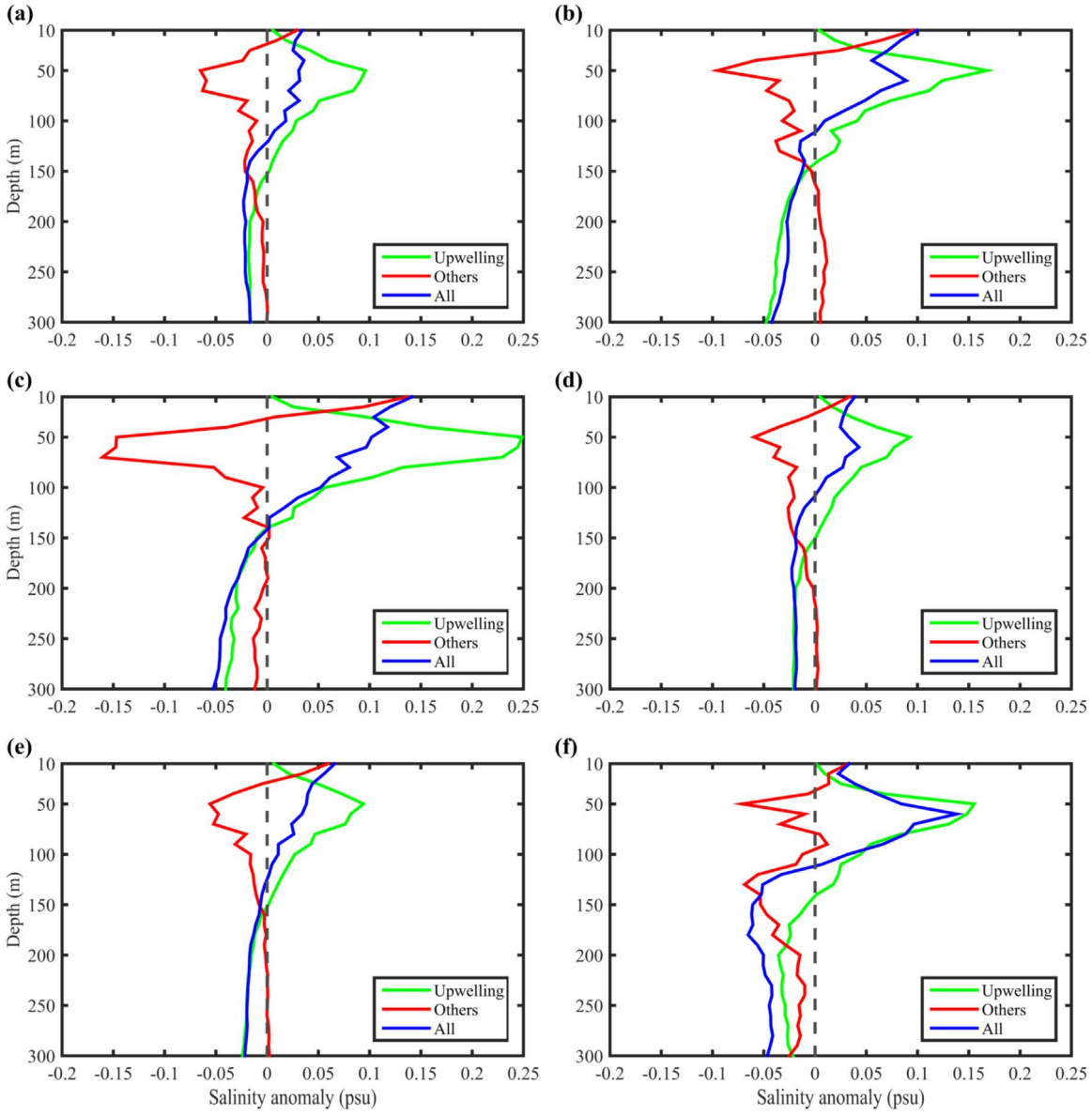

Fig. 10. Same as Fig. 9, but for salinity anomaly.

Table 1
Average values of maximum wind speed and translation speed for all categories of typhoons and corresponding pre-typhoon average MLDs.

	Average maximum wind speed ($m\ s^{-1}$)	**Average translation speed** ($m\ s^{-1}$)	**Average MLD** (m)
Weak typhoons	40.1	7.5	36.1
Strong typhoons	58.8	6.1	34.9
Slow-moving typhoons	47.1	3.1	35.4
Fast-moving typhoons	47.6	7.9	35.7
Typhoons above shallow ML	47.6	7.1	30.4
Typhoons above deep ML	47.1	6.0	59.2

typhoons, which can affect the ocean's response to a certain extent (Figs. 7d, e, 8d, and e). Mei et al. (2012) demonstrated that the climatological ML is deeper at low latitudes where typhoons often travel slowly, compared to those at high latitudes where typhoons often travel fast. The average latitude of typhoon centers above the deep ML is 16.77°N, while that above the shallow layer is 23.94°N. Table 1 shows that typhoons above the deep ML have a lower translation speed (6.0 m s^{-1}) on average than those above the shallow ML (7.3 m s^{-1}). These are in agreement with the results of Mei et al. (2012). As presented above, slowly moving typhoons tend to cause a stronger upwelling under the typhoon track. Here the former elevated the 14 °C isotherm 16.4 m, while the latter resulted in a 12.5 m upward shift. This partly explains why the subsurface negative temperature anomaly and positive salinity anomaly in the central water column are larger in the area with deep ML than their counterparts in the area with shallow ML. Additionally, the vertical temperature gradient in the subsurface layer is greater in the deep ML area than in the shallow ML area (Fig. 11), providing more favorable conditions for the appearance of a prominent negative temperature anomaly associated with upwelling in the subsurface layer of the former.

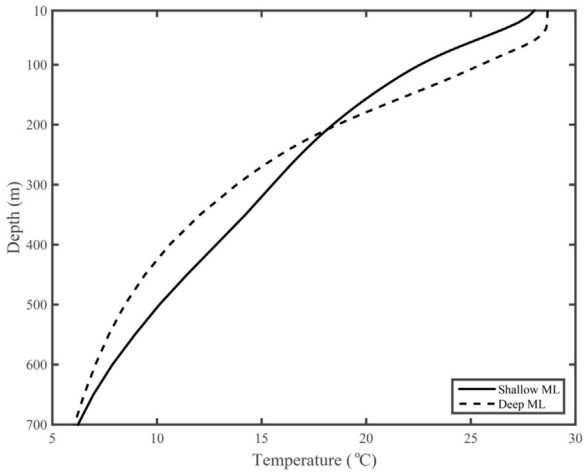

Fig. 11. The averaged temperature profiles with a shallow ML (solid curve) and with a deep ML (dashed curve) before the typhoon arrival.

Table 2
Dependence of oceanic responses on air-sea parameters. For each parameter, the results in the upper row are from this study and those in the lower row are from Price (1981). $\Delta\overline{SST}^{y}$ is the cross-track averaged ΔSST and in this study it was obtained within 100 km of the typhoon track.

Air-sea parameter	Value of parameter	$\frac{\partial\Delta\overline{SST}^{y}}{\partial()}$	$\frac{\partial\Delta SST_{\max}}{\partial()}$
Maximum wind speed	49 m s^{-1}	−0.03 °C m^{-1} s	−0.05 °C m^{-1} s
	35 m s^{-1}	−0.14 °C m^{-1} s	−0.24 °C m^{-1} s
Translation speed	5.7 m s^{-1}	0.25 °C m^{-1} s	0.32 °C m^{-1} s
	8.5 m s^{-1}	0.18 °C m^{-1} s	0.31 °C m^{-1} s
Initial MLD	36 m	0.03 °C m^{-1}	0.04 °C m^{-1}
	30 m	0.03 °C m^{-1}	0.06 °C m^{-1}

It is interesting that the subsurface positive temperature anomaly expected from vertical mixing is absent in the temperature anomaly profile induced by other factors in the area with deep ML (Fig. 9f). This indicates that the vertical mixing here may contribute little to the temperature anomaly. Another possible reason is that there must be more uncertainty in the cases with an initial deep ML since they have much less sampling profiles (33) than those (148) with an initial shallow ML.

To further examine ocean response varying with the typhoons' intensity (maximum wind speed) and translation speed as well as pre-typhoon (initial) MLD, we calculated the dependence of SST response on these air-sea parameters following Price (1981). Table 2 shows the comparison between the results from this study and those from Price (1981). For each varied parameter, the other parameters are fixed to given values in Price's numerical experiments while they are the mean values of all cases in this study, as shown in Table 2. The dependence of cross-track averaged SST anomaly ($\Delta\overline{SST}^{y}$) and maximum SST anomaly ($\Delta SST_{\max}$) on the parameters were determined from the classified composite results presented above, which is some different from more accurate determination in the numerical experiments. Notwithstanding these differences, present results are basically in agreement with Price's numerical results (Table 2). A large discrepancy appears in the dependence on maximum wind speed. In this study, the changes with maximum wind speed of both $\Delta\overline{SST}^{y}$ and $\Delta SST_{\max}$ are smaller by a factor of nearly 5 than the counterparts of the numerical results. This may be because the initial MLD (36 m) averaged from all cases is larger than that (30 m) adopted in the numerical experiments. Deep ML reduces the sensitivity of SST response to the maximum wind speed as Lloyd and Vecchi (2011) indicated that the regions with shallower ML have a greater sensitivity to wind forcing.

5. Summary and conclusions

The responses of ocean temperature and salinity to typhoons were analyzed using composite Argo float observations. The composite results are generally in agreement with previous numerical simulations, sea surface composite results from remote sensing data, and case studies. The magnitude of the temperature and salinity anomalies is sensitive to typhoon intensity, translation speed, and pre-typhoon MLD; however, the basic structures of these anomalies do not change much. The importance of upwelling, relative to other factors, in temperature and salinity anomalies induced by typhoons was roughly quantified.

While vertical mixing is well known to affect temperature and salinity responses to typhoons, upwelling also plays an important role in these responses. In general, the contribution of upwelling to the temperature anomaly within 75 km of a typhoon track is smaller in the surface layer but larger below than that of other factors. For the salinity anomaly, the upwelling is dominant except in the layers of 10–20 m and 110–160 m where the vertical salinity gradient is very weak. The upwelling induced by strong or slow-moving typhoons tends to generate larger temperature and salinity anomalies compared to weak or fast-moving typhoons. A thicker than normal ML reduces the effect of upwelling and vertical mixing on surface layer cooling but enhances the effect of upwelling on cooling below the ML.

Acknowledgments

This work was jointly funded by the National Research and Development Program of China (Grant no. 2016YFA0601103), the National Natural Science Foundation of China (Grants U1305231 and 41276007), one project from the State Key Laboratory of Satellite Ocean Environment Dynamics (Grant no. QNHX1612), and the President Research Award (2013121047). This study is a contribution to the international IMBER project. The Argo data were collected and made freely available by the International Argo Program and the national programs that contribute to it (http://www.argo.ucsd.edu, http://argo.jcommops.org). The Argo Program is part of the Global Ocean Observing System. The typhoon data are from the Joint Typhoon Warning Center (http://www.usno.navy.mil/JTWC), and the CARS2009 data from the Commonwealth Scientific and Industrial Research Organization (http://www.marine.csiro.au/atlas/). We thank Jim Price at WHOI and the other two anonymous reviewers for their helpful comments and suggestions on an earlier version of the manuscript.

References

Argo, 2000. Argo float data and metadata from Global Data Assembly Centre (Argo GDAC). Ifremer. ⟨http://doi.org/10.12770/1282383d-9b35-4eaa-a9d6-4b0c24c0cfc9⟩.
Bender, M.A., Ginis, I., Kurihara, Y., 1993. Numerical simulations of tropical cyclone-ocean interaction with a high-resolution coupled model. J. Geophys. Res. 98 (23), 245–263.
de Boyer Montégut, C., Madec, G., Fischer, A.S., Lazar, A., Iudicone, D., 2004. Mixed layer depth over the global ocean: an examination of profile data and a profile-based climatology. J. Geophys. Res. 109, C12003.
Brand, S., 1971. The effects on a tropical cyclone of cooler surface waters due to upwelling and mixing produced by a prior tropical cyclone. J. Appl. Meteorol. 10, 865–874.
Bueti, M.R., Ginis, I., Rothstein, L.M., Griffies, S.M., 2014. Tropical cyclone-induced thermocline warming and its regional and global impacts. J. Clim. 27, 6978–6999.
Cheng, L., Zhu, J., Sriver, R.L., 2015. Global representation of tropical cyclone-induced short-term ocean thermal changes using Argo data. Ocean Sci. 11, 719–741.
Chiang, T.L., Wu, C.R., Oey, L.Y., 2011. Typhoon Kai-Tak: an ocean's perfect storm. J. Phys. Oceanogr. 41, 221–233. http://dx.doi.org/10.1175/2010JPO4518.1.
D'Asaro, E.A., Sanford, T.B., Niiler, P.P., Terrill, E.J., 2007. Cold wake of Hurricane Frances. Geophys. Res. Lett. 34, L15609.
Dare, R.A., McBride, J.L., 2011. Sea surface temperature response to tropical cyclones. Mon. Weather Rev. 139, 3798–3808. http://dx.doi.org/10.1175/MWR-D-10-05019.1.
D'Asaro, E.A., et al., 2014. Impact of Typhoons on the Ocean in the Pacific. Bull. Am.

Meteorol. Soc. 95 (9), 1405–1418.
Emanuel, K.A., 1986. An air-sea interaction theory for tropical cyclones. Part I: steady-state maintenance. J. Atmos. Sci. 43, 585–605.
Emanuel, K.A., 2001. Contribution of tropical cyclones to meridional heat transport by the oceans. J. Geophys. Res. 106, 14771–14781. http://dx.doi.org/10.1029/2000JD900641.
Emanuel, K.A., DesAutels, C., Holloway, C., Korty, R., 2004. Environmental control of tropical cyclone intensity. J. Atmos. Sci. 61, 843–858.
Emery, W.J., Thomson, R.E., 2001. Data Analysis Methods in Physical Oceanography. Elsevier, New York.
Gandin, L.S., 1965. Objective Analysis of Meteorological Fields. Israel program for scientific translations, Jerusalem.
Hart, R.E., Maue, R.N., Watson, M.C., 2007. Estimating local memory of tropical cyclones through MPI anomaly evolution. Mon. Weather Rev. 135, 3990–4005. http://dx.doi.org/10.1175/2007MWR2038.1.
Huang, P., Sanford, T.B., Imberger, J., 2009. Heat and turbulent kinetic energy budgets for surface layer cooling induced by the passage of Hurricane Frances (2004). J. Geophys. Res. 114, C12023. http://dx.doi.org/10.1029/2009JC005603.
Large, W.G., McWilliams, J.C., Niiler, P.P., 1986. Upper ocean thermal response to strong autumnal forcing of the Northeast Pacific. J. Phys. Oceanogr. 16, 1524–1550.
Leipper, D.F., 1967. Observed ocean conditions and Hurricane Hilda, 1964. J. Atmos. Sci. 24, 182–186.
Lin, I.I., Wu, C.C., Pun, I.F., Ko, D.S., 2008. Upper-ocean thermal structure and the western North Pacific category 5 typhoons. Part I: Ocean features and the category 5 typhoons' intensification. Mon. Weather Rev. 136, 3288–3306. http://dx.doi.org/10.1175/2008MWR2277.1.
Liu, Z., Xu, J., Zhu, B., Sun, C., Zhang, L., 2007. The upper ocean response to tropical cyclones in the northwestern Pacific analyzed with Argo data. Chin. J. Oceanol. Limnol. 25, 123–131. http://dx.doi.org/10.1007/s00343-007-0123-8.
Lloyd, I.D., Vecchi, G.A., 2011. Observational evidence of oceanic controls on hurricane intensity. J. Clim. 24, 1138–1153. http://dx.doi.org/10.1175/2010JCLI3763.1.
Mei, W., Pasquero, C., 2012. Restratification of the upper ocean after the passage of a tropical cyclone: a numerical study. J. Phys. Oceanogr. 42, 1377–1401.
Mei, W., Pasquero, C., 2013. Spatial and temporal characterization of sea surface temperature response to tropical cyclones. J. Clim. 26 (11), 3745–3765. http://dx.doi.org/10.1175/JCLI-D-12-00125.1.
Mei, W., Pasquero, C., Primeau, F., 2012. The effect of translation speed upon the intensity of tropical cyclones over the tropical ocean. Geophys. Res. Lett. 39, L07801. http://dx.doi.org/10.1029/2011GL050765.
Mrvaljevic, R.K., et al., 2013. Observations of the cold wake of Typhoon Fanapi (2010). Geophys. Res. Lett. 40 (2), 316–321.
Park, J.J., Kwon, Y.-O., Price, J.F., 2011. Argo array observation of ocean heat content changes induced by tropical cyclones in the north Pacific. J. Geophys. Res. 116, C12025. http://dx.doi.org/10.1029/2011JC007165.
Park, J.J., Park, K.A., Kim, K., Youn, Y.H., 2005. Statistical analysis of upper ocean temperature response to typhoons from ARGO floats and satellite data. In: IGARSS'05 Proceedings, IEEE, Piscataway, New Jersey, pp. 2564–2567.
Price, J.F., 1981. Upper ocean response to a hurricane. J. Phys. Oceanogr. 11, 153–175.
Price, J.F., 1983. Internal wave wake of a moving storm. Part I. Scales, energy budget and observations. J. Phys. Oceanogr. 13 (6), 949–965.
Price, J.F., 2009. Metrics of hurricane-ocean interaction vertically-integrated or vertically-averaged ocean temperature. Ocean Sci. 5, 351–368.
Price, J.F., Sanford, T.B., Forristall, G.Z., 1994. Forced stage response to a moving hurricane. J. Phys. Oceanogr. 24, 233–260.
Price, J.F., Morzel, J., Niiler, P.P., 2008. Warming of SST in the cool wake of a moving hurricane. J. Geophys. Res. 113, C07010.
Riser, S.C., et al., 2016. Fifteen years of ocean observations with the global Argo array. Nat. Clim. Change 6, 145–153.
Sanford, T.B., Price, J.F., Girton, J.B., 2011. Upper ocean response to hurricane frances (2004) observed by profiling EM-APEX floats. J. Phys. Oceanogr. 41, 1041–4056. http://dx.doi.org/10.1175/2010JPO4313.1.
Siswanto, E., et al., 2008. Ocean physical and biogeochemical responses to the passage of Typhoon Meari in the East China Sea observed from Argo float and multiplatform satellites. Geophys. Res. Lett. 35 (15), L15604. http://dx.doi.org/10.1029/2008GL035040.
Vincent, E.M., et al., 2012b. Assessing the oceanic control on the amplitude of sea surface cooling induced by tropical cyclones. J. Geophys. Res. 117 (C5), C05023. http://dx.doi.org/10.1029/2011JC007705.
Vincent, E.M., Lengaigne, M., Madec, G., Vialard, J., Samson, G., Jourdain, N.C., Menkes, C.E., Jullien, S., 2012a. Processes setting the characteristics of sea surface cooling induced by tropical cyclones. J. Geophys. Res. 117, C02020. http://dx.doi.org/10.1029/2011JC007396.
Wingo, M.T., Cecil, D.J., 2010. Effects of vertical wind shear on tropical cyclone precipitation. Mon. Weather Rev. 138 (3), 645–662. http://dx.doi.org/10.1175/2009MWR2921.1.
Wu, C.C., Tu, W.T., Pun, I.F., Lin, I.I., Peng, M.S., 2016. Tropical cyclone-ocean interaction in Typhoon Megi - A synergy study based on ITOP observations and atmosphere- ocean coupled model simulations. J. Geophys. Res. Atmos. 121, 153–167.
Yablonsky, R.M., Ginis, I., 2009. Limitation of one-dimensional ocean models for coupled hurricane-ocean model forecasts. Mon. Weather Rev. 137, 4410–4419.
Zhang, W.Z., Lin, S., Jiang, X.M., 2016. Influence of tropical cyclones in the western North Pacific. In: Anthony, L. (Ed.), Recent Developments in Tropical Cyclone Dynamics, Prediction, and Detection. InTech, Croatia, EU (Austria), 3–24 http://dx.doi.org/10.5772/64009.